Progress In Electromagnetics Research Letters, Vol. 28, 195–205, 2012

COMPENSATION OF WAVE ATTENUATION IN LEFT-HANDED TRAVELING-WAVE FIELD-EFFECT TRANSISTORS

S. Nakagawa and K. Narahara*

Graduate School of Science and Engineering, Yamagata University, 4-3-16 Jonan, Yonezawa, Yamagata 992-8510, Japan

Abstract—We characterize left-handed (LH) traveling-wave field effect transistors (TWFETs), which consist of two composite right- and left-handed (CRLH) transmission lines that are electromagnetically coupled by capacitances, inductances, and FET transconductances, for obtaining loss-free LH waves. In a device, two different propagation modes can support LH waves. We find that one of these modes gain wave amplitudes, while the other loses them. This amplitude gain can compensate wave attenuation resulting from electrode loss and substrate leakage. This study clarifies which mode gains amplitudes and the method of matched terminations, together with several experimental observations that validate the design criteria.

1. INTRODUCTION

Composite right- and left-handed (CRLH) transmission lines have been investigated for practical use of left-handed (LH) waves. They have been successfully applied to microwave applications such as couplers [1, 2], oscillators [3], and compact antennas for cellphones [4, 5]. By dimensional extensions, CRLH lines can provide high-resolution lenses with no aberrations [6, 7].

However, the use of CRLH lines is sometimes limited because of wave attenuation caused by finite electrode resistance and substrate current leakage. To widen the application area of CRLH lines, some scheme of loss compensation must be introduced. Si et al. proposed a method of loss compensation, which employs negative resistances realized by FET pairs in each cell of CRLH lines [8]. Casares-Miranda et al. introduced interconnecting amplifiers in several pieces of CRLH

Received 15 October 2011, Accepted 22 December 2011, Scheduled 29 December 2011
* Corresponding author: Koichi Narahara (narahara@yz.yamagata-u.ac.jp).

lines [9]. Our scheme is based on traveling-wave field-effect transistors (TWFETs), whose gate and drain lines have a CRLH line structure, hereafter called LHTWFETs for brevity. Because of the resonance caused by inductance-capacitance (LC) pairs that are included in the CRLH structure, unless the line is carefully designed, autonomous oscillation dominates such that the left-handedness is completely lost. We recently derived the conditions for suppressing autonomous oscillations by analyzing complex dispersion [10]. Moreover, this study describes the design criteria for obtaining loss-free LH waves in LHTWFETs. We consider the case when all the series inductances are negligible for convenience. Owing to the presence of capacitive and inductive couplings between the gate and drain lines, two different propagation modes can support LH waves. It is found that only one of the two modes can gain the amplitudes of supporting LH waves, while the other mode attenuates them. When an LHTWFET is excited by the gain mode and terminated with the characteristic impedance of the corresponding mode, we succeed in obtaining loss-free or amplified LH waves without multiple reflections.

We discuss the design criteria for loss-free LH waves after mentioning the fundamental properties of LHTWFETs, including the structure, equivalent circuit, and dispersion. We then describe experimental observations. For definite validations, we employ a standard breadboard and perform the experiments at MHz frequencies; this frequency is much smaller than the microwave frequencies at which CRLH lines are extensively used. As a result, we can fix erroneous operations by reforming the test line and easily detect voltage at any cells.

2. DESIGN CRITERIA FOR LOSS-FREE LH WAVES IN LHTWFETS

Figure 1 shows a sample structure of the unit cell of an LHTWFET. Both the active and passive elements are mounted on the front surface, while the back surface is for the ground metal connected with the source electrode of every FET. We consider a case when the series inductances of both gate and drain lines are negligible for convenience, such that both the gate and drain lines consist of $C_{Lg(d)}$, $C_{Rg(d)}$, and $L_{Lg(d)}$. The gate and drain lines are coupled via C_m. Moreover, these two lines are coupled via FET contributions. The gate and drain lines are periodically connected with the gate and drain electrodes, which are labeled as G and D in Fig. 1, respectively.

Figures 2(a) and (b) show the circuit configuration and the equivalent representation of the unit cell of the line, respectively. The

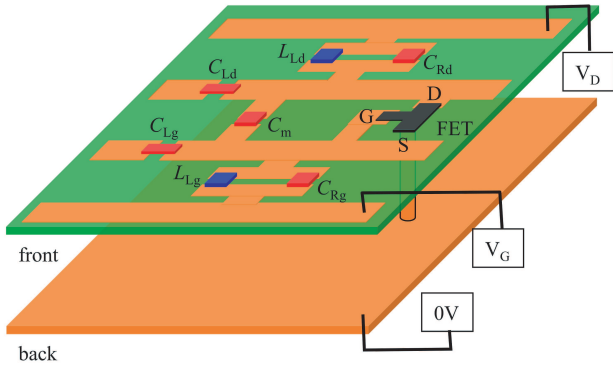

Figure 1. Structure of the unit cell of an LHTWFET. This sample can be developed by the two-layer print-circuit-board. The drain, gate, and source electrodes of an FET are labelled as D, G, and S, respectively.

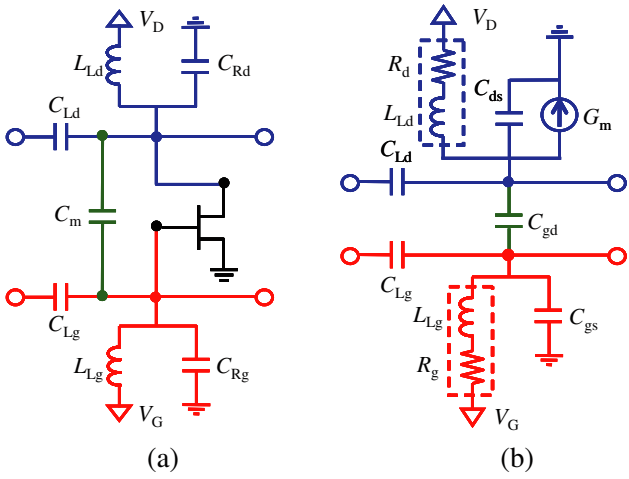

Figure 2. Representation of the unit cell of an LHTWFET. (a) The circuit configuration and (b) the equivalent representation of an LHTWFET.

red, blue, and green symbols represent the gate line, drain line, and electromagnetic coupling, respectively. The parasitic gate-source, gate-drain, and drain-source capacitances of an FET can be simply added to C_{Rg}, C_m, and C_{Rd}, respectively, resulting in C_{gs}, C_{gd}, and C_{ds}, respectively. The finite resistances, R_g and R_d, are accompanied by the inductors, L_{Lg} and L_{Ld}, respectively. The FET drain–source current

is modelled by the transconductance G_m. The transmission equations are given by

$$\frac{d}{dt}(V_{n-1} - V_n) = \frac{I_n}{C_{Lg}}, \tag{1}$$

$$\frac{d}{dt}(W_{n-1} - W_n) = \frac{J_n}{C_{Ld}}, \tag{2}$$

$$\begin{aligned} &\frac{d}{dt}\left(I_n - I_{n+1}\right) + \frac{R_{Lg}}{L_{Lg}}\left(I_n - I_{n+1}\right) \\ &= \frac{V_n}{L_{Lg}} + C_g\left(\frac{R_{Lg}}{L_{Lg}}\frac{dV_n}{dt} + \frac{d^2V_n}{dt^2}\right) - C_{gd}\left(\frac{d^2W_n}{dt^2} + \frac{R_{Lg}}{L_{Lg}}\frac{dW_n}{dt}\right), \end{aligned} \tag{3}$$

$$\begin{aligned} &\frac{d}{dt}\left(J_n - J_{n+1}\right) + \frac{R_{Ld}}{L_{Ld}}\left(J_n - J_{n+1}\right) \\ &= G_m\left(\frac{R_{Ld}}{L_{Ld}}V_n + \frac{dV_n}{dt}\right) - C_{gd}\left(\frac{R_{Ld}}{L_{Ld}}\frac{dV_n}{dt} + \frac{d^2V_n}{dt^2}\right) + \frac{W_n}{L_{Ld}} \\ &\quad + C_d\left(\frac{R_{Ld}}{L_{Ld}}\frac{dW_n}{dt} + \frac{d^2W_n}{dt^2}\right), \end{aligned} \tag{4}$$

where V_n, W_n, I_n, and J_n are the gate voltage at the nth node, drain voltage at the nth node, gate current at the nth section, and drain current at the nth section, respectively. Here, we define $C_g \equiv C_{gs} + C_{gd}$ and $C_d \equiv C_{ds} + C_{gd}$.

Owing to the couplings between the gate and drain lines, there are two different propagation modes that mostly develop at a given frequency. To understand this more clearly, we first derive the dispersion relationship of an LHTWFET without considering the transconductance. Substituting $\exp(i\omega t + ikn)$ into the spatiotemporal dependences of the voltages and currents and applying the long-wavelength approximation, i.e., $\exp(\pm k) \sim 1 \pm k$, the wave number k is given for the angular frequency ω as

$$k(\omega) = \sqrt{\frac{x_1 + x_2 \pm \sqrt{(x_1 - x_2)^2 - 4C_{gd}^2 L_{Lg} L_{Ld} \omega^2 x_3}}{2x_3}}, \tag{5}$$

Table 1. Line parameters used to obtain Fig. 3.

C_{Lg} (pF)	470.0	C_{gs} (pF)	47.0
L_{Lg} (μH)	10.0	C_{ds} (pF)	470.0
C_{Ld} (pF)	470.0	C_{gd} (pF)	47.0
L_{Ld} (μH)	4.7		

where

$$x_1 = C_{Lg}L_{Lg}\left(1 - C_dL_{Ld}\omega^2\right), \tag{6}$$

$$x_2 = C_{Ld}L_{Ld}\left(1 - C_gL_{Lg}\omega^2\right), \tag{7}$$

$$x_3 = C_{Lg}C_{Ld}L_{Lg}L_{Ld}\omega^2. \tag{8}$$

We can see that two different wave numbers can satisfy Eq. (5), each of which corresponds to the mode that supports waves in an LHTWEFT. For definiteness, we call the fast and slow modes as the π- and c-modes, respectively; therefore, the dispersion having the upper (lower) sign is for the c- (π-) mode, which is denoted as $k_{c(\pi)}(\omega)$. Fig. 3 shows the typical dispersion relationship of an LHTWFET. Table 1 shows the parameters we employ. The red and blue curves represent the c- and π-modes, respectively. Note that both modes exhibit left-handedness.

Each mode has its own voltage fraction (drain voltage/gate voltage) between the lines and characteristic impedances. Let the voltage fraction of the c- (π-) modes be $R_{c(\pi)}$, then we obtain

$$R_{c,\pi}(\omega) = \frac{x_1 - x_2 \pm\sqrt{(x_1 - x_2)^2 + 4x_3C_m^2L_{Lg}L_{Ld}\omega^2}}{2C_mC_{Ld}L_{Lg}L_{Ld}\omega^2}. \tag{9}$$

In general, R_c is positive and R_π is negative, so that the c-mode has the same parity between the gate and drain lines, and the π-mode has the opposite parity. By setting the fraction of the input sinusoidal waves applied at the gate and drain lines to $R_{c(\pi)}$, we can develop the waves supported uniquely by the c- or the π-mode. On the other hand, the characteristic impedance is respectively given for the gate and drain lines as

$$Z_{cg,\pi g}(\omega) = \frac{1}{k_{c,\pi}(\omega)\omega C_{Lg}}, \tag{10}$$

$$Z_{cd,\pi d}(\omega) = \frac{1}{k_{c,\pi}(\omega)\omega C_{Ld}}. \tag{11}$$

Once we succeed in wave propagation by the unique mode, multiple reflections can be suppressed by terminating the gate and drain lines with the characteristic impedances of the corresponding mode.

Next, we consider the effects of transconductance on these modes. Under small presence of parasitic resistances and transconductances, the dispersion relationship becomes complex: $k'_{c(\pi)} \equiv k_{c,\pi}(\omega) + i\alpha_{c,\pi}$. Obviously, the waves supported by the c- (π-) mode can gain

amplitudes, if $\alpha_{c(\pi)} > 0$. By straightforward calculations, we obtain

$$\begin{aligned}
\alpha_c \;=\; & \frac{C_{gd} v_c G_m}{2C_{Lg}C_{Ld}\omega^4(1/v_c^2 - 1/v_\pi^2)} \\
& + \frac{v_c\left[-x_1 + x_2 + \omega^2\left(1/v_c^2 - 1/v_\pi^2\right)x_3\right] R_{Lg}}{4C_{Lg}L_{Lg}^2\omega^4\left(1/v_c^2 - 1/v_\pi^2\right)x_3} \\
& + \frac{v_c\left[x_1 - x_2 + \omega^2\left(1/v_c^2 - 1/v_\pi^2\right)x_3\right] R_{Ld}}{4C_{Ld}L_{Ld}^2\omega^4\left(1/v_c^2 - 1/v_\pi^2\right)x_3}, \qquad (12) \\
\alpha_\pi \;=\; & -\frac{C_{gd} v_\pi G_m}{2C_{Lg}C_{Ld}\omega^4\left(1/v_c^2 - 1/v_\pi^2\right)} \\
& + \frac{\left[x_1 - x_2 + \omega^2\left(1/v_c^2 - 1/v_\pi^2\right)x_3\right] R_{Lg}}{2C_{Lg}L_{Lg}^2\omega^4(1/v_c^2 - 1/v_\pi^2)[x_1 + x_2 - \omega^2(1/v_c^2 - 1/v_\pi^2)x_3]v_\pi} \\
& + \frac{\left[-x_1 + x_2 + \omega^2\left(1/v_c^2 - 1/v_\pi^2\right)x_3\right] R_{Ld}}{2C_{Ld}L_{Ld}^2\omega^4(1/v_c^2 - 1/v_\pi^2)[x_1 + x_2 - \omega^2(1/v_c^2 - 1/v_\pi^2)x_3]v_\pi}, \qquad (13)
\end{aligned}$$

where $v_{c(\pi)}$ represents $\omega/k_{c(\pi)}$. Moreover, the upper (lower) signs are for the c- (π-) mode.The second and third terms on the right hand side of Eqs. (12) and (13) represent the contributions of the loss elements, such that they are always shown to be negative. Because v_π is always larger than v_c by definition, the first term on the right hand side is also negative in Eq. (12); therefore, α_c is always negative, i.e., the c-mode cannot contribute to loss-free wave propagation. On the other hand, α_π can become zero or positive. It is thus concluded that the π-mode can uniquely support non-attenuated LH waves.

Because of the factor $(1/v_c^2 - 1/v_\pi^2)$ in the denominator of the G_m term, it is effective to minimize the discrepancy between v_c and v_π at a given frequency in order to obtain the maximal gain. One convenient method to establish this criterion is to design line parameters in such a way that the two dispersion curves have a cross-point without C_m. For the completely uncoupled case, two modes represent the waves traveling in either the gate or drain line. For the gate mode, the frequencies corresponding to $k = 0$ and $k = \pi$ are given in rad/cell by $\omega_{ug} \equiv 1/\sqrt{C_{gs}L_{Lg}}$ and $\omega_{lg} \equiv 1/\sqrt{(C_{gs} + 4C_{Lg})L_{Lg}}$, respectively. For the drain mode, the corresponding two frequencies are given by $\omega_{ud} \equiv 1/\sqrt{C_{ds}L_{Ld}}$ and $\omega_{ud} \equiv 1/\sqrt{(C_{ds} + 4C_{Ld})L_{Ld}}$. Fig. 4 shows the situation for the case when ω_{ug} is greater than ω_{ud}. The blue and red curves represent the gate and drain modes, respectively. When there is a cross-point, we only require the condition $(\omega_{ug} - \omega_{ud})(\omega_{lg} - \omega_{ld}) < 0$. Note that the LHTWFET with parameters listed in Table 1 satisfies this condition. Moreover, the discrepancy between v_c and v_π becomes minimal at 2.54 MHz.

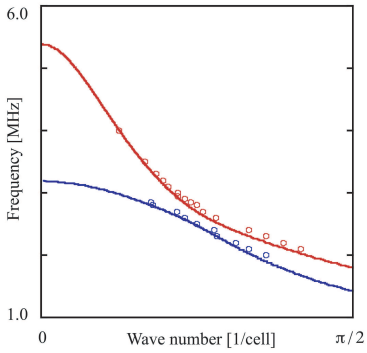

Figure 3. Dispersion relationship of an LHTWEFT. Parameter values are listed in Table 1. Red and blue curves are for the c- and π-modes, respectively. Points shown by the circles result from the standing-wave measurements.

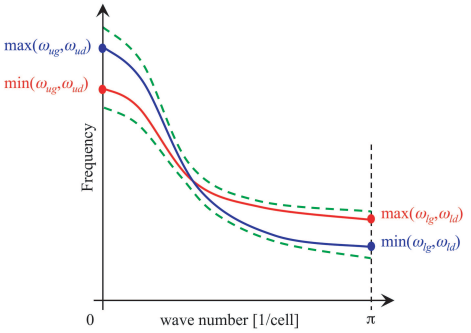

Figure 4. Dispersive property for maximal gain. ω_{ug} is assumed to be greater than ω_{ud}. Blue and red curves represent the gate and drain modes, respectively. The dashed curve represents the coupled-mode counterpart.

3. EXPERIMENTAL EVALUATIONS

We built a test LHTWFET using discrete components on a standard breadboard. We used a 90-section device whose unit cell is shown in Fig. 2. The transistors used were of the type TOSHIBA 2SK30A, with the threshold voltage $V_{TO} = -1.8\,\mathrm{V}$. Throughout the measurements, V_D was fixed at 2.0 V. The inductors and capacitors were implemented using the TDK-SPT0406 series and the TDK-FK series, respectively. Same values were set for capacitances and inductances, as seen in Table 1. The gate and drain lines were fed by the signals generated by a NF-WF1974 two-channel function generator. For evaluating the properties of the c- (π-) mode, the input voltage fraction between the gate and drain lines channels of the input signal was set to $R_{c(\pi)}$. The waveforms were detected by Agilent 10073C passive probes and monitored in the time domain by using an Agilent DSO90254A oscilloscope.

To examine whether the test circuit really simulates an LHTWFET, we evaluate the dispersion relationship of the test circuit. We set $V_G = -2.0\,\mathrm{V}$ ($< V_{TO}$) to disable the FET contributions. One end of the test circuit was fed by sinusoidal waves, and the other end was opened. We measured the separation between two adjacent nodes

of the resulting standing wave to identify with the half wavelength. By varying the input frequency, we can obtain the dispersion relationship of the test circuit. The results are shown in Fig. 3. The red and blue circles represent the experimental observations for the c- and π-modes, respectively. Good similarity is established between the calculated and measured results; therefore, the test circuit simulates our target well.

We evaluate the FET contributions to the waves in the test circuit. Gaussian envelope pulses with a carrier frequency of 2.5 MHz are input at one of the ends. At this frequency, R_c and R_π are calculated to be 1.43 and -0.70 , respectively. The other ends are terminated with Tyco-CFR16J series resistors matched with the π-mode characteristic impedances. Figs. 5(a) and (b) show the measured waveforms of the c-mode inputs monitored at $n = 10$ and $n = 40$ for $V_G = -2.0\,\mathrm{V}$ ($< V_{TO}$) and $V_G = -1.17\,\mathrm{V}$ ($> V_{TO}$), respectively. Note that the gate and drain waveforms have a common parity. The red and blue waveforms represent the waveforms monitored on the gate and drain lines, respectively. Because of the parasitic resistances of L_{Lg} and L_{Ld}, the pulses are simply attenuated in Fig. 5(a). As suggested in Eq. (12), the FET attenuates the pulses even more in Fig. 5(b). Similar waveforms for the π-mode inputs are shown in Fig. 6. For the pinch-off case, the amplitudes of the pulses decrease in Fig. 6(a) similar to that for the c-mode. Moreover, the amplitude gain by the FET contribution is established in Fig. 6(b). It is thus concluded that the π-mode gains the amplitude of the supporting waves, while the c-mode waves are attenuated. Fig. 7 shows four subsequent spatial waveforms for the π-

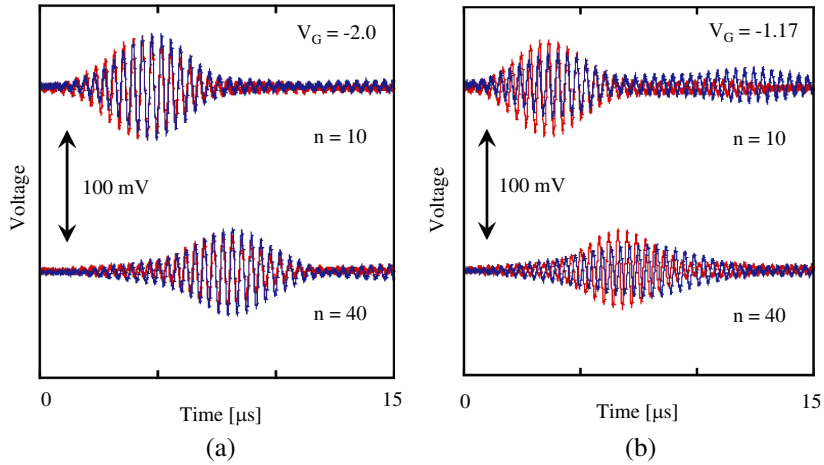

Figure 5. Measured time-domain waveforms of the c-mode monitored at $n = 10$ and $n = 40$. Red and blue waveforms correspond to the gate and drain lines, respectively. (a) $V_G < V_{TO}$ and (b) $V_G > V_{TO}$.

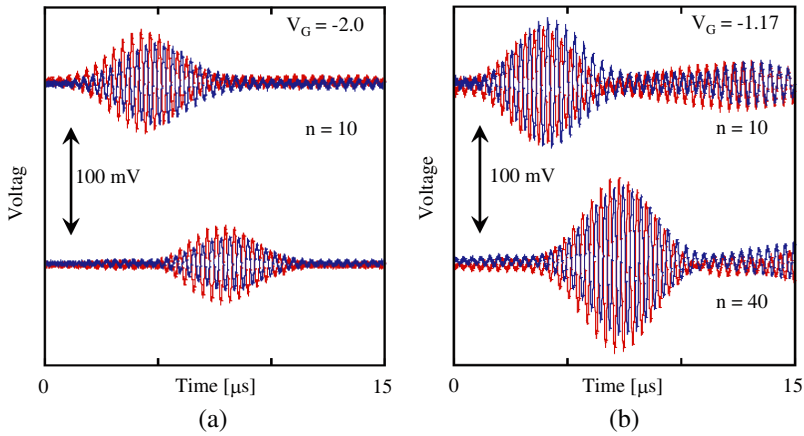

Figure 6. Measured time-domain waveforms of π-mode monitored at $n = 10$ and $n = 40$. Red and blue waveforms correspond to the gate and drain lines, respectively. (a) $V_G < V_{TO}$ and (b) $V_G > V_{TO}$.

mode pulse in the gate line at $V_G > V_{TO}$ with increments of 30 ns. They are numbered in the order of increasing time. Because the refractive index becomes negative, the phase travels oppositely to the power in the left-handed lines. We can see in Fig. 7 that the envelope travels to the right, while the phase travels to the left; therefore, the amplified waves exhibit left-handedness.

Figure 8 shows the frequency dependence of the per-unit-cell gain at $V_G = -1.17$ V. The solid curves represent the calculated dependence using Eqs. (12) and (13). To best fit the experimental results, we set R_{Lg}, R_{Ld}, and G_m to 4.0 Ω, 3.2 Ω, and 1.2 mS, respectively. The gain becomes maximal at the frequency where the discrepancy between v_c and v_π becomes minimal. The circles represent the measured results. To obtain these results, we compare the peak amplitude at $n = 20$ with that at $n = 10$ for the carrier frequencies ranging from 2.0 MHz to 3.0 MHz with increments of 0.1 MHz. For lower frequencies, the c-mode pulse is significantly influenced by dispersive distortions. In addition, a small but finite π-mode pulse superposes it; therefore, we cannot specify the per-unit-cell gain for the c-mode at frequencies less than 2.5 MHz. Through the measurements, we can see that the π-mode pulse experiences the maximal gain at 2.7 MHz, whereas the c-mode pulses are mostly attenuated. The discrepancy of the maximum-gain frequencies between the calculated and measured values may stem from capacitive contributions of FETs that are not considered in the design parameters. There is some optimal frequency that gives maximal gain to the π-mode pulse. Thus, it is strongly suggested to minimize the discrepancy between v_c and v_π at the design frequency.

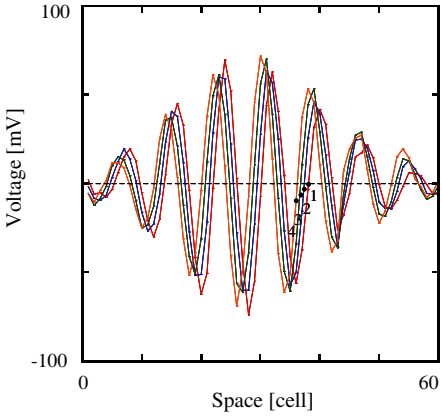

Figure 7. Four spatial waveforms of the π-mode pulse on the gate line at $V_G > V_{TO}$. The temporal increments are 30 ns. The waveforms are numbered in the order of increasing time; therefore, the phase travels to the left.

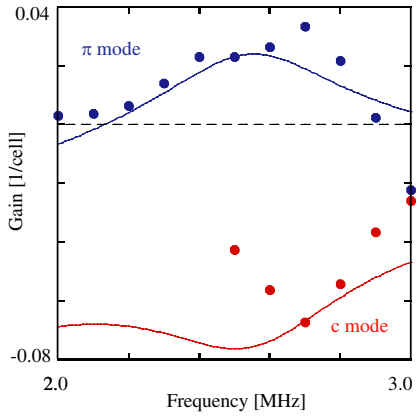

Figure 8. Frequency dependence of per-unit-cell gain. Solid curves represent the calculated dependence, while circles represent the experimentally obtained dependence.

4. CONCLUSION

We discuss the characteristics of waves propagating along LHTWFETs. There are two different modes that support LH waves, called the c- and π-modes, both of which exhibit left-handedness. We found that the π-mode gains amplitudes, while the c-mode loses them. When the LHTWFET is terminated with the π-mode characteristic impedance, the multiple reflections of waves can be effectively suppressed. These observations are successfully validated by several experimental investigations using a test LHTWFET. The design criteria we develop are equally applied not only to the present MHz circuits but also to the microwave circuits, when the cell structure shown in Fig. 2 is well developed. Further studies may significantly widen the scope of the application of LH waves, including the introduction of series inductors and dimensional extensions.

REFERENCES

1. Caloz, C., A. Sanada, and T. Itoh, "A novel composite right/left-handed coupled-line directional coupler with arbitrary coupling

level and broad bandwidth," *IEEE Trans. Microwave Theory Tech.*, Vol. 52, No. 3, 980–992, March 2004.

2. Caloz, C. and H. V. Nguyen, "Novel broadband conventional and dual-composite right/left-handed (C/D-CRLH) metamaterials: Properties, implementation and double-band coupler application," *Appl. Physics A*, Vol. 87, No. 2, 309–316, May 2007.
3. Kim, Y.-H., J. Choi, and C. Seo, "Dual-band push-push OSC using CRLH transmission line and tunable negative resistance based on pin diode," *Microw. and Optical Tech. Lett.*, Vol. 53, No. 7, July 2011.
4. Gummalla, A., C.-J. Lee, and M. Achour, "Compact metamaterial quadband antenna for mobile application," *IEEE Int. Symp. Antenna Propag.*, San Diego, CA, 2008.
5. Huang, W., N. Xu, V. Pathak, G. Poilasne, and M. Achour, "Composite right-left handed metamaterial ultra-wideband antenna," *IEEE International Workshop on Antenna Technology*, 1–4, March 2–4, 2009.
6. Pendry, J. B., "Negative refraction makes a perfect lens," *Phys. Rev. Lett.*, Vol. 85, 3966–3969, 2000.
7. Grbic, A. and G. V. Eleftheriades, "Overcoming the diffraction limit with a planar left-handed transmission-line lens," *Phys. Rev. Lett.*, Vol. 92, 117403-1–117403-4, March 2004.
8. Si, L.-M., T. Jiang, K. Chang, X. Lv, L. Ran, and H. Xin, "Active microwave metamaterials incorporating ideal gain devices," *Materials*, Vol. 4, No. 1, 73–83, Jan. 2010.
9. Casares-Miranda, F. P., C. Camacho-Penalosa, and C. Caloz, "High-gain active composite right/left-handed leaky-wave antenna," *IEEE Trans. Antennas Propagat.*, Vol. 54, No. 8, 2292–2300, August 2006.
10. Nakagawa, S. and K. Narahara, "Characterization of lefthanded traveling-wave transistors," *IEICE Trans. Electron.*, Vol. E92-C, No. 11, 1396–1400, 2009.